J. Fluid Mech. (1996), vol. 320, pp. 117–137

Evolution of patterns of streamwise vorticity in the turbulent near wake of a circular cylinder

By C. CHYU AND D. ROCKWELL

Department of Mechanical Engineering and Mechanics, Lehigh University, Bethlehem, PA 18015, USA

(Received 16 May 1995 and in revised form 27 March 1996)

High-image-density particle image velocimetry allows characterization of the instantaneous patterns of streamwise vorticity ω_x over the cross-section of the near wake of a circular cylinder, and the manner in which they evolve with streamwise distance. Emphasis is on the Reynolds number $Re = 10 \times 10^3$, for which the Kelvin–Helmholtz (K–H) mode in the separating shear layers has a streamwise wavelength much smaller than that of the Kármán mode. Consequently, the corresponding spanwise wavelength between ω_x concentrations increases substantially from its value in the separating shear layer to a larger one in the near wake. This streamwise evolution is defined by spatial correlations of patterns of instantaneous ω_x and interpreted with the aid of the quasi-two-dimensional topology of the wake in the base region of the cylinder. The principal features of the phase-averaged topology are foci of the initially formed Kármán vortices and a saddle point between them. Immediately downstream of this saddle, remarkably coherent patterns of ω_x concentrations are evident; they have a wavelength approximately equal to the cylinder diameter. Moreover, larger-scale spanwise distortion eventually occurs. This distortion exhibits several modes; the most severe is a nearly discontinuous variation of patterns of ω_x.

1. Introduction

Even at relatively low values of Reynolds number, of the order of a few hundred, the near wake of a circular cylinder exhibits remarkable complexity, evident in the early investigation of Hama (1957), who visualized the three-dimensional distortion of the Kármán vortices. More recently, Gerrard (1978), Williamson (1988, 1992), König, Eisenlohr & Eckelmann (1993), and Zhang *et al.* (1995) have characterized the detailed structure of the three-dimensionality in the near wake; a central ingredient of this structure is the development of streamwise vortices between the Kármán vortices. Williamson (1996) has provided an overall assessment of this complex three-dimensionality.

Very recent studies of the near-wake structure have focused on the predominant spanwise lengthscales up to Reynolds numbers of the order of 2000. Mansy, Yang & Williams (1994) employed laser scanning anemometry and Wu *et al.* (1994*b*) used digitized hydrogen bubble markers to show that the spanwise wavelength, which is of the order of the cylinder diameter, generally exhibits a decrease with increasing Reynolds number.

At sufficiently high values of Reynolds number, of the order of 10^3, the structure of the very near wake is complicated by the onset of a Kelvin–Helmholtz (K–H) instability in the separating shear layer. It has come to be known as the Bloor–Gerrard instability or transition wave, originally investigated by Bloor (1964) and Gerrard

(1978), and more recently by Wei & Smith (1986), Kourta *et al.* (1987), Unal & Rockwell (1988), Bays-Muchmore & Ahmed (1993), Filler, Marston & Mih (1991), and Sheridan *et al.* (1993). These investigations have employed a variety of visualization approaches to demonstrate that the small-scale concentrations of vorticity arising from the K–H instability exhibit ordered quasi-two-dimensional and three-dimensional patterns along the separated shear layer up to a Reynolds number of at least 20×10^3. The scale of, and wavelength between, these concentrations of vorticity decreases with increasing Reynolds number. Correspondingly, their characteristic frequency increases. These aspects have been addressed by Bloor (1964), Wei & Smith (1986), Kourta *et al.* (1987), Filler *et al.* (1991), Sheridan *et al.* (1993), Yokoi & Kamemoto (1992, 1993) and Wu *et al.* (1994*d*). Quantitative imaging of the instantaneous structure of the K–H and Kármán vortices is given by Lin, Towfighi & Rockwell (1995).

The near wake of the cylinder therefore exhibits two characteristic lengthscales, one associated with the streamwise wavelengths between the Kelvin–Helmholtz vortices and the other between the Kármán vortices. It follows that two distinct spanwise wavelengths λ_z may occur. This issue is assessed by Williamson, Wu & Sheridan (1995) on the basis of the flow visualization, scanning laser measurements of Mansy *et al.* (1994), and particle image velocimetry measurements of Rockwell & Lin (1993), Wu *et al.* (1994*a*), and Lin, Vorobieff & Rockwell (1994, 1995).

The large number of investigations on mixing layers from thin splitter plates is directly relevant to our considerations of the shear layer instability, i.e. the Kelvin–Helmholtz instability. Detailed assessments of the quasi-two-dimensional and three-dimensional features of such mixing layers, which are beyond the scope of the present summary, are provided by Roshko (1976), Ho & Huerre (1994), Hussain (1986), Huang & Ho (1990), Bell & Mehta (1992). The onset of spanwise non-uniformity in mixing layers was indicated in the early studies of Brown & Roshko (1974), Konrad (1976), and Breidenthal (1981). By visualizing the cross-section of this class of flows, Bernal & Roshko (1986), and Jimenez, Cogolos & Bernal (1985) demonstrated the existence of streamwise vorticity concentrations. The mechanism giving rise to this three-dimensionality was elucidated by Corcos & Lin (1984), Lasheras, Cho & Maxworthy (1986), and Lasheras & Choi (1988) as vortex stretching in the braid region between the quasi-two-dimensional spanwise vortices. Huang & Ho (1990) show that the spanwise wavelength rapidly decreases in the streamwise (x) direction until, near the onset of the first vortex merging, it tends towards an asymptotic value of $\lambda_z/\lambda_x = 2/3$. It is therefore crucial that any scaling of spanwise to streamwise wavelength properly accounts for the dimensionless streamwise distance at which the flow is characterized, emphasized by Huang & Ho to be Rx/λ_o, in which R is the velocity ratio across the mixing layer and λ_o is the reference wavelength of λ_x.

For flow past a cylinder, at relatively high Reynolds numbers over the range from 5×10^3 to 20×10^3, the quasi-two-dimensional wavelength of the Kármán and Kelvin–Helmholtz vortices are sharply differentiated, the latter being an order of magnitude smaller than the former. Very little attention has been given to the structure and scaling of the small-scale streamwise vortices corresponding to the K–H and Kármán modes in the very near wake, prior to and during onset of the first Kármán vortex. Previous investigations of Hayakawa & Hussain (1989) and Bays-Muchmore & Ahmed (1993), extending over $3 \leqslant x/D \leqslant 40$, in which x is the distance downstream of the cylinder, indicate that the spanwise scale λ_z appears to be of the order of one cylinder diameter D. The investigations of Rockwell & Lin (1993) and Lin *et al.* (1994, 1995) have focused on the location $x/D = 1$ in the very near wake where the first Kármán vortex forms; they find $\lambda_z/D \sim 1$. The evolution of the patterns of streamwise

vorticity ω_x along the near wake has remained uninvestigated, and the transformation from patterns of ω_x associated with the K–H mode to those linked to the Kármán mode remains unclarified.

These three-dimensional features of the wake at higher values of Reynolds number are, of course, related to the time-averaged characterizations of three-dimensionality of Szepessy & Bearman (1992) and Norberg (1994). Szepessy & Bearman investigated the effects of aspect ratio and end plates on spanwise correlations of velocity and pressure in the near wake; in addition, spectra and instantaneous time traces of pressure and velocity were acquired along the span. Spanwise variation of the phase of Kármán vortex shedding was clearly evident; their correlation measurements suggest a spanwise scale of the order of $2.5D$. Norberg (1994), in a complementary study of the effects of aspect ratio and end conditions, found a strong dependence of the spanwise scale, of the order of $5D$ to $15D$, on Reynolds number. These time-averaged studies suggest the possibility of instantaneous, large-scale distortions along the span of the near wake.

The present study employs instantaneous concentrations of streamwise vorticity as a means to characterize the predominant instantaneous scales and wavelengths of the three-dimensionality of the near wake. The feasibility of this approach has been demonstrated through characterization of instantaneous vorticity distributions from stationary and oscillating plain cylinders, in addition to cylinders having localized and distributed non-uniformities, mostly at much lower values of Reynolds number than addressed herein, as described by Rockwell *et al.* (1992, 1993), Rockwell & Lin (1993), Towfighi & Rockwell (1994), Wu *et al.* (1994*a*, *b*). These investigations have revealed various features of vorticity concentrations orthogonal to those of the primary Kármán vortices. By use of cinema techniques, it is possible to construct three-dimensional space–time images of the near wake, as demonstrated by Rockwell & Lin (1993), Lin & Rockwell (1994), Lin, Vorobieff & Rockwell (1993, 1995). Instantaneous values of circulation associated with the streamwise vorticity concentrations and related features of the near-wake vorticity field at a single location ($x/D = 1$) in the near wake are addressed by Lin *et al.* (1995).

Consideration of the near-wake structure at high Reynolds number leads to a number of unclarified issues. Recognizing that there are two predominant scales of quasi-two-dimensional vortices in the near wake, the K–H and Kármán vortices, and accounting for the rapid onset of the K–H vortices immediately downstream of separation, it is expected that the patterns of instantaneous streamwise vorticity will exhibit substantial variations along the wake in the streamwise direction. Yet, virtually no quantitative insight is available on the streamwise variation of the instantaneous vorticity concentrations. In addition, there is a tendency to characterize the spanwise lengthscale of the three-dimensionality in terms of a single wavelength λ_z. However, the complex three-dimensional distortion mechanisms in the near wake at high Reynolds number are expected to give rise to staggered, rather than in-line concentrations of streamwise vorticity, i.e. a cross-stream wavelength λ_y of significant magnitude is expected. A further feature of the near wake is the existence of a separating shear layer along the relatively low-velocity region adjacent to the base of the cylinder, which is influenced by the downstream development of the large-scale Kármán vortices. Characterization of λ_z in relation to the structure of this region has remained unexplored. Finally, the possible existence of large-scale spanwise distortions, having lengthscales substantially larger than the λ_z between vorticity concentrations, may exert an important influence on the overall mechanism of Kármán shedding. The structure of these distortions may be related to vortex dislocations observed at much lower values of Reynolds number. The manner in which such large-scale distortions

alter the patterns of streamwise vorticity concentrations associated with the K–H and Kármán instabilities, as well as generating new concentrations of their own, remains unclarified. This investigation addresses these complex features of the near-wake structure.

2. Flow system and experimental techniques

All experiments were performed in a large-scale free-surface water channel having a test section 914 mm wide, 597 mm high, and 4880 mm long. The water level was maintained at a depth of 540 mm. The test section was preceded by a large-scale 2:1 contraction, preceded by a honeycomb-screen conditioning system, which provided a free-stream uniformity within 0.5% and turbulence intensity less than 0.1% The flow velocity was maintained at 183 mm s^{-1}. This speed, in conjunction with cylinder diameters of 25 and 51 mm, yielded Reynolds numbers based on diameter D, of 5×10^3 and 10×10^3. For brevity, nearly all of the data presented herein are at $Re = 10 \times 10^3$. A full set of images at both Re is given by Chyu (1995). The Plexiglas cylinders were polished to a very smooth finish and had diameter variations of less than $0.002D$. They were mounted vertically in the water channel and bounded by end plates as indicated in figure 1, such that the values of aspect ratio were $L/D = 18$ and 9 respectively. These end plates had a diameter of 254 mm, a thickness of 5 mm, and were bevelled at a sharp angle of 15° on the exterior side. The same principal features of the flow structure were observed for these two different cylinder systems.

High-image-density particle image velocimetry (PIV) was employed to determine the instantaneous velocity field over the cross-section of the wake. As indicated in the field of view of figure 1, this approach led to instantaneous concentrations of streamwise vorticity ω_x. The general technique involved a scanning-laser version of PIV, as described Rockwell *et al.* (1993), Rockwell (1993), Rockwell & Lin (1993), Towfighi & Rockwell (1994), and Lin *et al.* (1995). A brief summary of the overall approach is given here. The (y, z)-plane of figure 1, indicated as the field of view in the plane of the laser sheet, was defined by a scanning beam from a 4 W continuous wavelength Argon–ion laser, which was focused on a rotating, polygonal mirror having 72 facets. The scanning frequency of the laser beam was 626 cycles s^{-1}. This approach provides, in essence, a pulsed laser sheet having a thickness of 1 mm, as assessed in detail by Rockwell *et al.* (1993). The camera shutter was maintained open for several scans of the laser beam, generating multiply-exposed images of each of the 14 μm metallic-coated particles in the flow. The field of view indicated in figure 1 was transmitted to the exterior of the test section by means of an image steering mirror, oriented at 45° with respect to the free stream. This technique is described in detail by Lin & Rockwell (1994). The centre of this mirror was placed at a minimum distance $x/D = 9.5$ downstream of the cylinder, such that the dynamics of the near wake were not influenced, as verified by hydrogen bubble and particle tracking videos. Outside the test section of the water channel, the particle images were reflected against an image shifting mirror, which imparted a constant bias displacement to all particle images, thereby precluding difficulties associated with directional ambiguity and large dynamic range across the extent of the field of view. Images were recorded by a Nikon F4 camera using high-resolution film (300 lines mm^{-1}); the lens had a magnification of 1:5. The 35 mm negative was then digitized using a digitizer having a resolution of 125 pixels mm^{-1}. This field of digitized particle images was subjected to a single-frame cross-correlation technique, based on the concept of Meinhart, Prasad & Adrian (1992), yielding the velocity field at each location of the interrogation window having

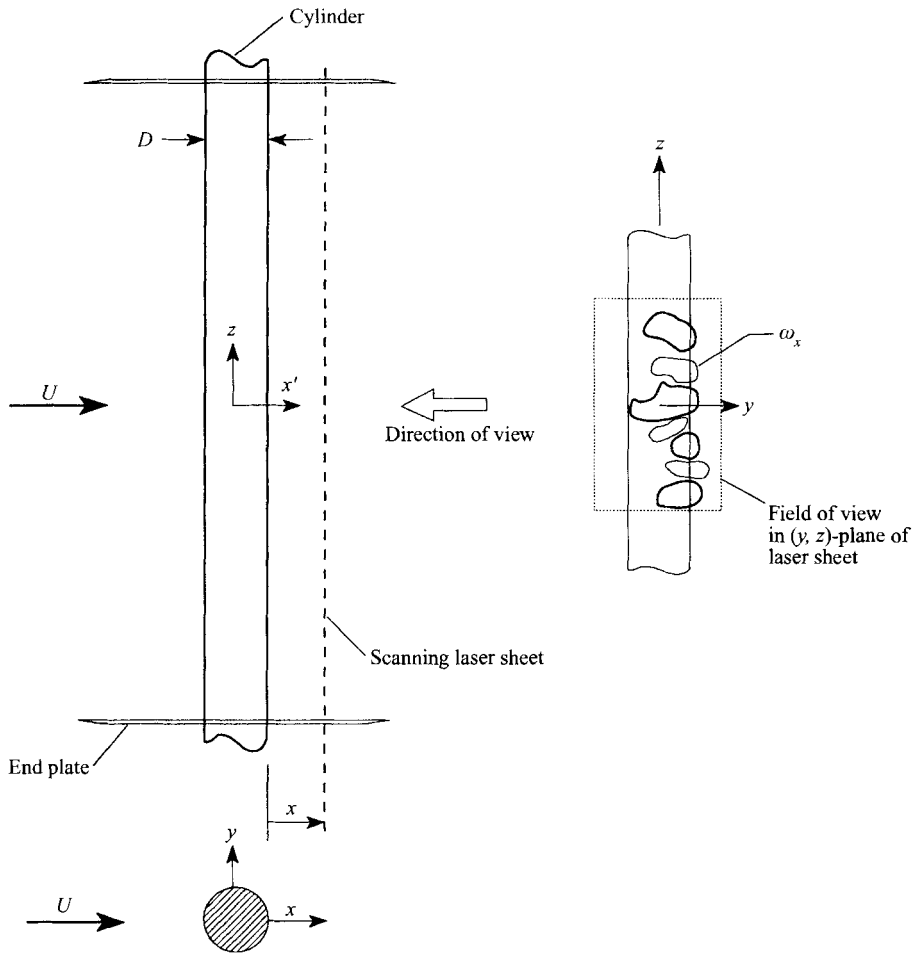

FIGURE 1. Schematic of experimental system.

dimensions of 100 pixels by 100 pixels. Interrogation areas were overlapped by 50%. The effective grid size on the plane of the film was 0.4 mm. The values of spatial resolution in the plan of the laser sheet, relative to the cylinders of diameter $D = 25$ and 51 mm, were therefore $0.08D$ and $0.04D$ respectively.

Both instantaneous and averaged PIV images are employed to represent the flow structure. Averaged images were determined from instantaneous ones that were randomly acquired at arbitrary phases during the Kármán cycle of oscillation. In contrast to phase-locked image acquisition, this approach does not give flow structure unique to a specific phase of the Kármán vortex formation. Moreover, N images, ranging from $N = 5$ to 33, were employed for averaging; the value of N is specified for each set of averages. The object of these averages was to demonstrate the lack of phase-coherent non-stationary behaviour of the pattern of streamwise vorticity.

Regarding the uncertainties of the quantitative parameters determined from the instantaneous and averaged images, the upper uncertainty bound on the lengthscales L corresponding to the distance between vorticity concentrations is estimated to be 6%. This value compares with the uncertainties of local velocity and vorticity of 0.4% and 3% respectively.

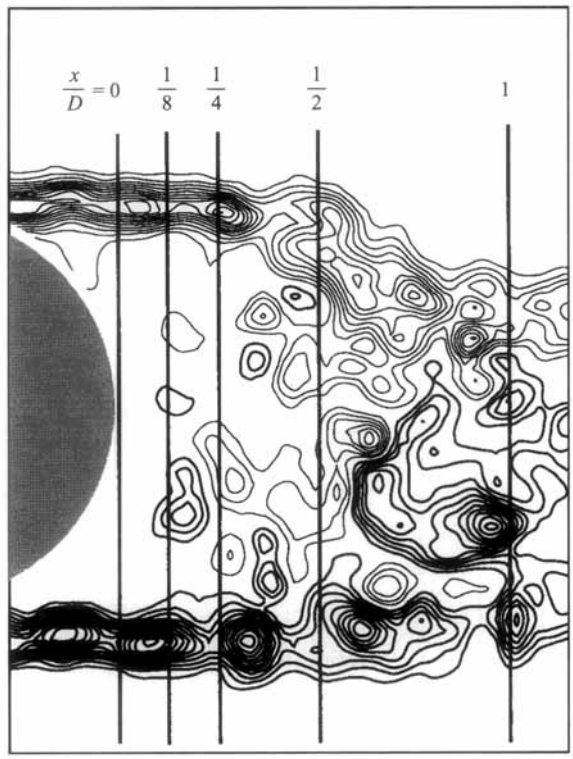

FIGURE 2. Quasi-two-dimensional view of instantaneous near-wake structure at $Re = 10 \times 10^3$ showing locations of cross-flow planes defined by laser sheet. Minimum and incremental vorticity levels are $|\omega_{min}| = 5\ s^{-1}$ and $\Delta\omega = 5\ s^{-1}$.

FIGURE 3. Instantaneous streamwise vorticity ω_x ($|\omega_{min}| = 5\ s^{-1}$, $\Delta\omega = 5\ s^{-1}$) and root-mean-square of fluctuating vorticity $\tilde{\omega}_{rms}$($\tilde{\omega}_{min} = 5\ s^{-1}$, $\Delta\tilde{\omega} = 1\ s^{-1}$) at $x/D = 0$. $Re = 10 \times 10^3$.

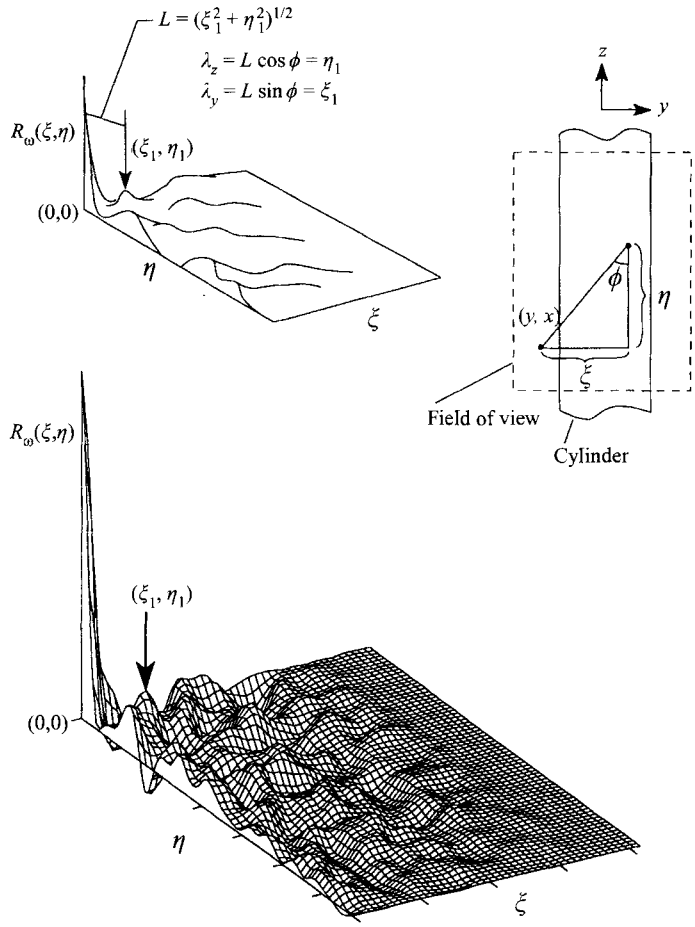

FIGURE 4. Vorticity correlation function $R_\omega(\xi, \eta)$ of instantaneous streamwise vorticity field ω_x at $x/D = 0$. $Re = 10 \times 10^3$.

3. Patterns of streamwise vorticity in the very near wake

The field of view of the cross-flow plane of the near wake, corresponding to images of instantaneous velocity and streamwise vorticity ω_x, is shown in figure 1 and described in further detail in §2. It is insightful to relate these cross-flow images to the corresponding, quasi-two-dimensional patterns. Figure 2 shows quasi-two-dimensional images of vorticity at $Re = 10 \times 10^3$. The streamwise locations x/D of the cross-flow planes are designated as vertical lines; these lines are superposed on contours of constant spanwise vorticity ω_z in the (x, y)-plane. The images of instantaneous ω_z show small-scale K–H vortices in the separating shear layers. Pronounced concentrations of ω_x occur at locations close to and upstream of the base, i.e. upstream of $x/D = 0$. We therefore expect the corresponding manifestations of three-dimensionality to be detectable in the cross-flow plane at $x/D = 0$. For the particular instantaneous image shown at $Re = 10 \times 10^3$, the pattern of small-scale vortices sets in much earlier in the lower shear layer from the cylinder. Examination of a sequence of instantaneous images revealed that this pattern switches between the upper and lower layers, in general accord with, but not phase-locked to, the formation of the Kármán vortices. At the instant shown, more pronounced three-dimensionality is therefore expected to occur in the shear layer from the lower side of the cylinder, and distributions of ω_x on

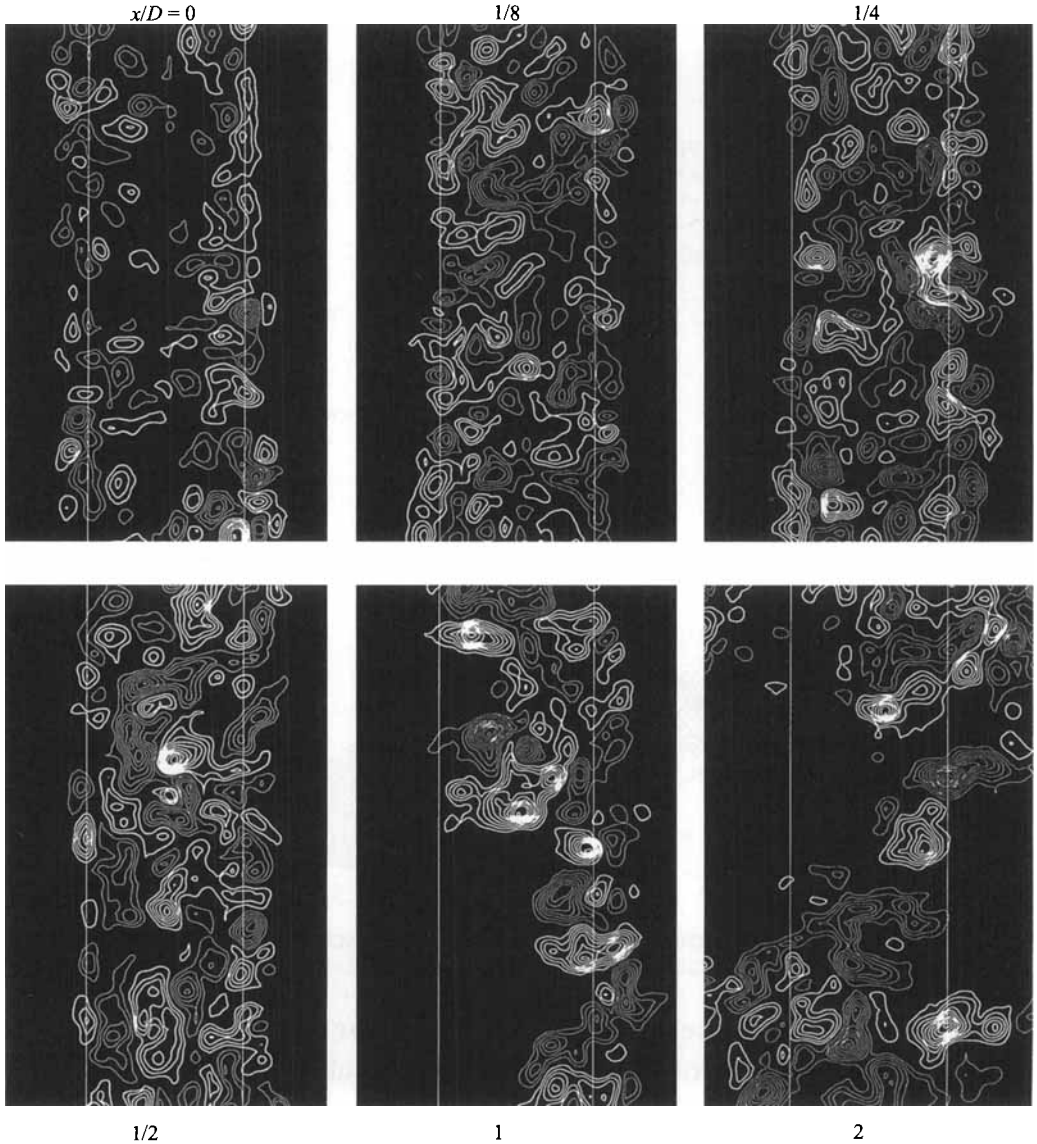

FIGURE 5. Streamwise development of ω_x for $Re = 10 \times 10^3$. Minimum contour level $|\omega_{min}| = 5\ s^{-1}$, contour increment $\Delta\omega = 5\ s^{-1}$.

the cross-flow plane will exhibit higher levels in that region. Regarding the onset of Kármán vortex formation at $Re = 10 \times 10^3$, the centre of the large-scale concentration of vorticity formed from the lower surface of the cylinder is at $x/D \approx 0.9$. The streamwise location of the onset of both the K–H and Kármán vortices is not stationary: it fluctuates up- and downstream of the nominal locations shown in figure 2, evident from examination of a number of instantaneous images.

Figure 3 shows a comparison of a representative image of instantaneous vorticity ω_x and the root-mean-square of the fluctuating vorticity $\tilde{\omega}_{rms}$ over the (y, z) cross-flow plane at $x/D = 0$ for $Re = 10 \times 10^3$. The instantaneous concentrations ω_x tend to be centred on the projected boundaries of the cylinder designated by the thin white vertical lines. The pattern centred on the right-hand boundary exhibits highly

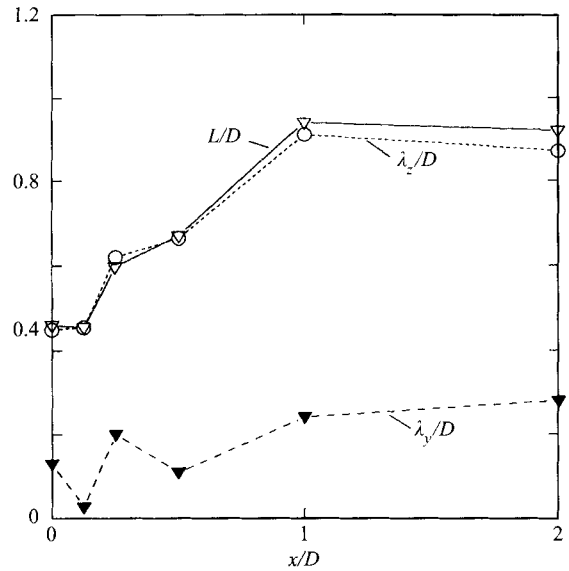

FIGURE 6. Averaged spanwise and cross-flow wavelength of ω_x concentrations as a function of x/D. $Re = 10 \times 10^3$.

concentrated vorticity, while that on the left-hand boundary shows lower-level, irregular distributions of vorticity. This pronounced asymmetry of patterns of ω_x concentrations is due to the different maturity of the small-scale quasi-two-dimensional vortices, as described in conjunction with figure 2. The concentrations of ω_x on the right-hand side of the image are not arranged in-line with alternating sign, which is the traditionally accepted view for very low values of Reynolds number. Rather, this staggered quasi-ordered pattern of ω_x has the basic features of the initially formed pattern in a mixing layer at high Reynolds number, investigated by Bell & Mehta (1992).

The root-mean-square of the fluctuating vorticity was calculated according to the following equation:

$$\tilde{\omega}_{rms} = \left\{ \frac{1}{N-1} \sum_{i=1}^{N} [\omega_i - \bar{\omega}]^2 \right\}^{1/2}. \tag{1}$$

A total of 33 instantaneous images of ω_x, i.e. ω_i, was employed to determine the averaged $\bar{\omega}$ and $\tilde{\omega}_{rms}$ distributions. The intent of these $\tilde{\omega}_{rms}$ distributions is not to provide asymptotic statistical values; rather, it is to emphasize the non-stationary nature of the instantaneous ω_x. If they were to occur at the same locations in a sequence of images, the locations and peak values of $\tilde{\omega}_{rms}$ would approximate those of the ω_x image. This is clearly not the case, and we therefore conclude that the patterns of ω_x exhibit significant variations with time. A further observation is that the highest levels of $\tilde{\omega}_{rms}$ occur in the separating shear layers from the cylinder; that is they tend to be centred on the projections of the cylinder boundaries.

It is evident that determination of the representative wavelengths λ_z and λ_y along and normal to the span of the cylinder requires quantitative evaluation of patterns of instantaneous vorticity. The correlation of the instantaneous vorticity ω_x over the (y, z) cross-flow plane is defined as

$$R_\omega(\xi, \eta) = \frac{\langle \omega_x(y, z)\, \omega_x(y+\xi, z+\eta) \rangle_{sp}}{\omega_{rms}^2}, \tag{2}$$

in which ξ and η are variables of integration, corresponding to the distance from the designated point (y, z) in the (y, z)-plane to the point of interest in the (y, z)-plane, and ω_{rms} is the spatial root-mean-square of vorticity over the (y, z)-plane, which is used to normalize $R_\omega(\xi, \eta)$ to unity at $(\xi, \eta) = (0, 0)$. Figure 4 shows the $R_\omega(\xi, \eta)$ plot for the left-hand image of figure 3. The width and length of the $R_\omega(\xi, \eta)$ plot are the same as the corresponding crossflow (y, z) plane shown in figure 3. Also shown in figure 4 is the correlation length L, defined as the distance between the origin $(\xi, \eta) = (0, 0)$ and the first peak closest to the origin. Interpretation of the $R_\omega(\xi, \eta)$ plot and the use of this plot for estimating wavelengths λ_z and λ_y is discussed in detail by Chyu (1995). As illustrated in figure 4, L represents the shortest distance between correlated vorticity concentrations, which is then taken as the resultant wavelength of the vortical structure on the (y, z)-plane. The projection of L on the η-axis, i.e. $\eta_1 = L\cos\phi$, ϕ being the angle to the η-axis, gives the spanwise wavelength λ_z; similarly $\xi_1 = L\sin\phi$ represents cross-stream wavelength λ_y. On the basis of the first peak of $R_\omega(\xi, \eta)$, obtained from ten instantaneous images, the spacing of the small-scale concentrations of ω_x has an average dimensionless value of $L/D = 0.46$, whereas the average spanwise and cross-stream wavelengths are $\lambda_z/D = 0.45$ and $\lambda_y/D = 0.1$. From quasi-two-dimensional instantaneous images of the same case at $Re = 10 \times 10^3$, it was found that the average streamwise spacing λ_x between spanwise K–H vorticity concentrations ω_z is $\lambda_z/D = 0.24$. Therefore, the ratio of the spanwise to streamwise spacing of the small-scale structures is $\lambda_z/\lambda_x = 1.9$. This ratio is in general agreement with that expected from studies of mixing layers, at locations upstream of the first merging of adjacent spanwise vortices. Huang & Ho (1990) determined that $\lambda_z/\lambda_x = 1.65$ at the streamwise location where (y, z) structure was first detectable. Furthermore, Bell & Mehta (1992) found, during the initial stage of development of a mixing layer, that $\lambda_z/\lambda_x \approx 2$. Based on the experimental findings of Huang & Ho (1990), λ_z/λ_x tends to the asymptotic value of approximately 2.3 at locations further downstream. The essential ingredient for approaching this asymptotic value is, however, merging of adjacent spanwise vortices, an event that was undetected herein for the separating shear layers from the cylinder.

4. Streamwise development of patterns of streamwise vorticity

The evolution of the patterns of instantaneous ω_x in the streamwise direction is shown in figure 5. The minimum and incremental values of vorticity were maintained constant for all values of x/D. This allows comparison, from one value of x/D to the next, of the peak vorticity levels and circulation of vorticity concentrations. In all cases, instantaneous images were acquired at a phase when the patterns of ω_x are approximately centred on the cylinder axis. At larger values of x/D, patterns of ω_x are swept back and forth across the wake in accord with formation of the Kármán vortices. Only images corresponding to a nominal position midway between the extreme positions of the translating patterns are shown in figure 5.

The image at $x/D = 0$ shows small-scale concentrations of vorticity, which are generally located on the projected boundaries of the cylinder. On the other hand, at $x/D = 1/8$, $1/4$ and $1/2$, well-defined concentrations of vorticity exist over the entire cross-section of the wake. It is evident that the small-scale concentrations seen in the separating shear layers at $x/D = 0$ no longer exist in isolation at $x/D \geqslant 1/8$; rather, they are modulated by the vorticity in the base region, whose origin will be addressed in § 5. At $x/D = 1$, large-scale distortion of the pattern of well-defined ω_x concentrations sets in; it exhibits a remarkably abrupt change in the location of the large-scale ω_x

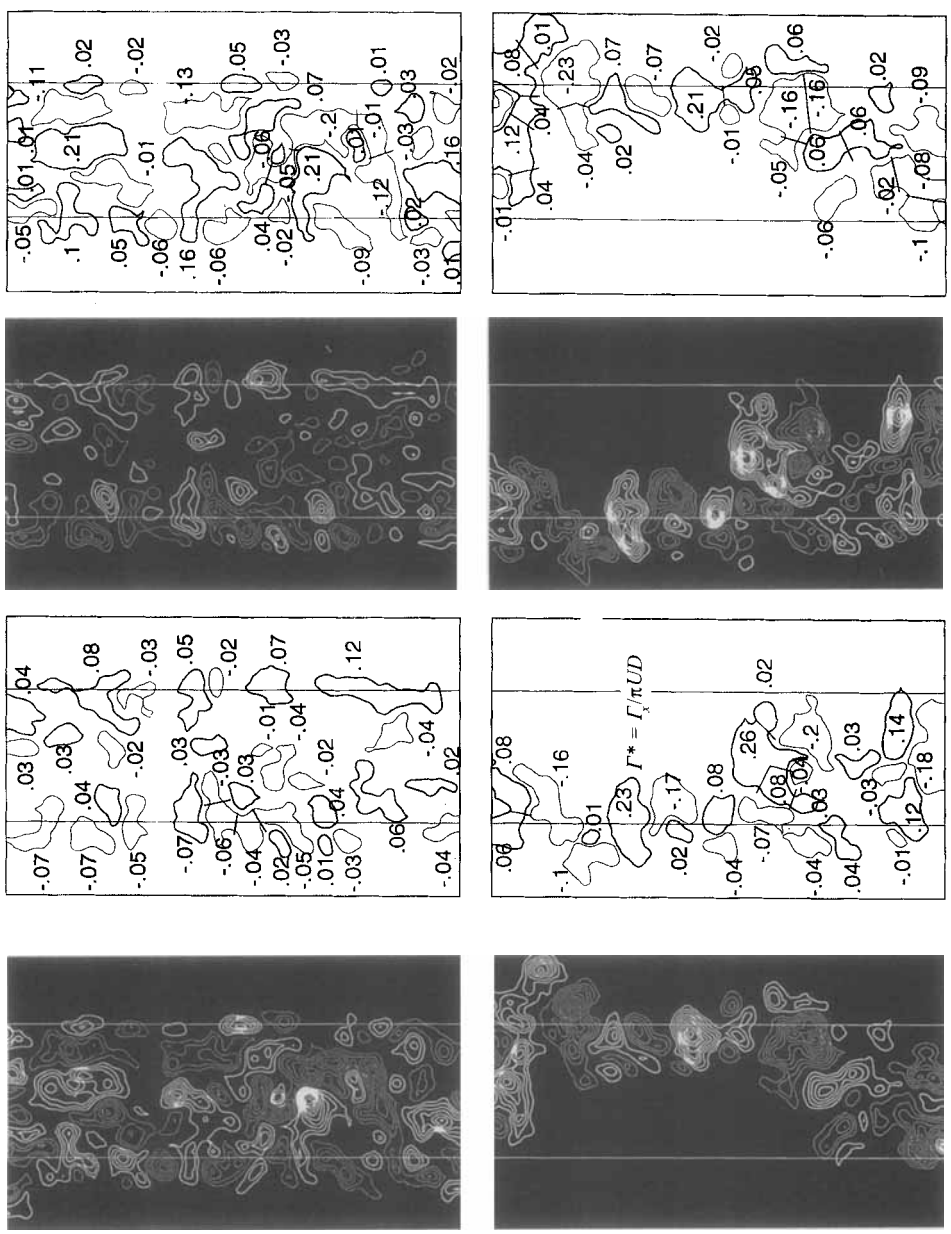

FIGURE 7. Dimensionless circulation $\Gamma_x/\pi UD$ corresponding to streamwise vorticity ω_x. $Re = 10 \times 10^3$. Minimum vorticity $|\omega_{min}| = 5\ s^{-1}$, contour increment $\Delta\omega = 5\ s^{-1}$.

concentrations. They are aligned with the centre of the cylinder over the top half of the image and with the right-hand side of the cylinder in the bottom half. This onset of large-scale distortion at $x/D = 1$ is in accord with the onset of formation of the quasi-two-dimensional Kármán vortex shown in figure 2. At $x/D = 2$ in figure 5, the large-scale distortion of the patterns of streamwise vorticity again shows a nearly discontinuous form. Further interpretation of these patterns, along with the corresponding velocity fields, will be addressed in §6.

In order to determine the representative spanwise λ_z and cross-stream λ_y wavelengths of the concentrations of ω_x, instantaneous vorticity correlations were calculated using the same approach as described in §3. At each value of x/D shown in figure 6, a total of five instantaneous images yielded an average value of resultant wavelength L and the corresponding spanwise λ_z and cross-stream λ_y wavelengths. The wavelengths λ_z/D nearly doubles from its initial value of $\lambda_z/D = 0.45$ at $x/D = 0$ to its essentially asymptotic values of $\lambda_z/D = 0.91$ and 0.88 at $x/D = 1$ and 2. Important is the observation that the value of λ_y/D is a substantial fraction of λ_z/D, emphasizing the necessity of simultaneously characterizing values of both λ_z and λ_y. As described by Chyu (1995), similar observations hold for $Re = 5 \times 10^3$. At this value of Re, however, the value of λ_y/λ_z can be as large as 0.45.

At a substantially lower value of Reynolds number $Re = 600$, Mansy *et al.* determined values of λ_z/D as a function of x/D using scanning LDA. The general form of their plot is remarkably similar to that of figure 6. The first detectable values of λ_z/D in their measurements, however, are further downstream relative to the values of figure 6, apparently due to the larger wavelengths of the K–H instability at lower Reynolds number.

5. Circulation of concentrations of streamwise vorticity

The dimensionless circulation $\Gamma^* \equiv \Gamma_x/\pi UD$ of the concentrations of ω_x were evaluated for representative instantaneous images. Γ_x is the normalized value of the streamwise circulation and U is the free-stream velocity. Values of Γ^* are given in figure 7. Each closed contour corresponding to the lowest level of vorticity served as the circuit for evaluating the circulation. In cases where these minimum levels of vorticity encompass two or more concentrations of vorticity, the closed vorticity contour is cut at the location indicated by a short straight line, in order to give an indication of the typical circulation of a single concentration of vorticity. The average value of Γ^* was determined by averaging all of the indicated Γ^* within each instantaneous image. Depending upon the image, the average involves 20–30 instantaneous Γ^*.

Figure 7 shows that Γ^* increases with x/D and attains average and maximum values of 0.06 and 0.26 at $x/D = 1$. The highest values of Γ^* are attained in the region corresponding to the onset and development of the large-scale Kármán vortex formation (compare figure 2).

6. Classification of large-scale modes of wake distortion

In the foregoing sections, the patterns of vorticity concentrations were captured at an instant when they were nominally centred on the axis of the cylinder. In this section, we broaden our consideration to include successive instants during the Kármán cycle of vortex formation, in order to allow definition of possible large-scale modes near and at the onset of the first Kármán vortex.

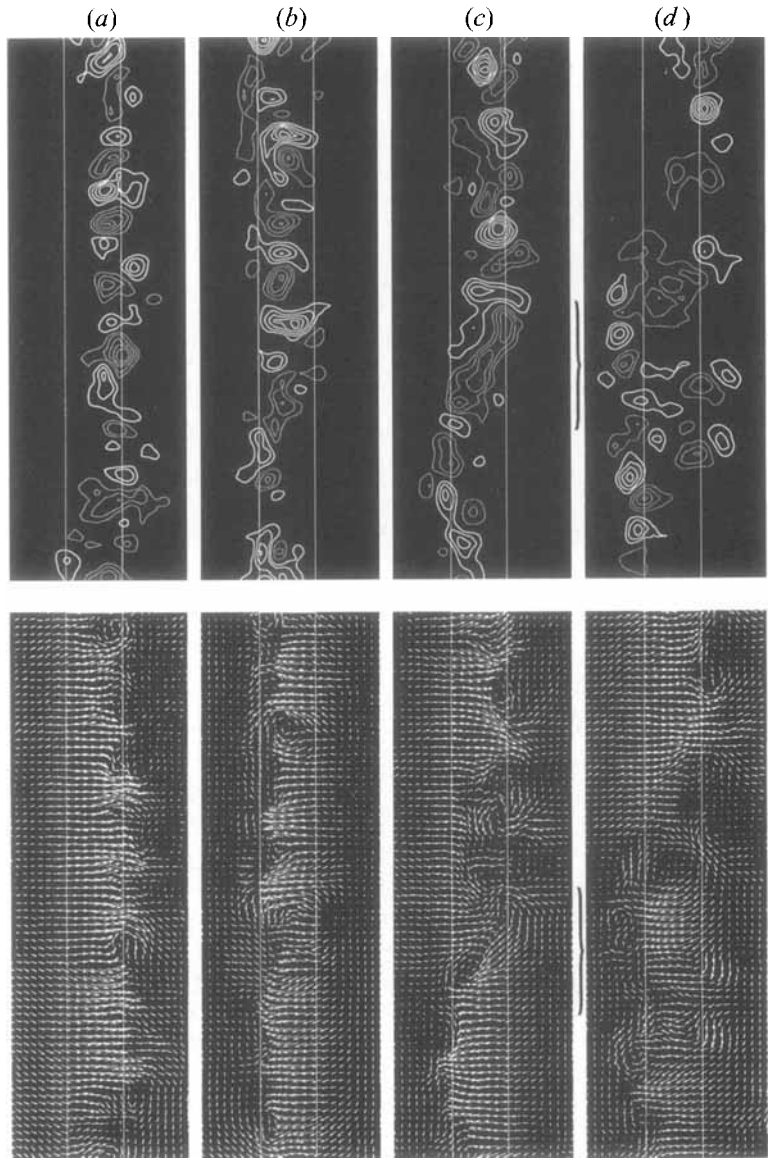

FIGURE 8. Streamwise vorticity and velocity fields near and after Kármán vortex formation. $Re = 5 \times 10^3$. Minimum vorticity contour level $|\omega_{min}| = 5\ s^{-1}$, contour increment $\Delta\omega = 5\ s^{-1}$. Images (*a*)–(*c*) are at $x/D = 1$; (*d*) is at $x/D = 2$.

At smaller values of x/D, well upstream of the location where Kármán vortex formation occurs, the patterns of vorticity remain confined between the essentially undeflected shear layers originating from the surfaces of the cylinder, as emphasized in images $1/8 \leqslant x/D \leqslant 1/2$ of figure 5. In this case, the approximate boundaries of the vorticity patterns correspond to the projections of the cylinder boundary. As shown by Chyu (1995), the patterns of velocity vectors suggest eddy-like structures corresponding to the vorticity concentrations. There is, however, no preferred orientation of the velocity vectors in the horizontal direction, which would suggest sweeping of the flow across the wake region, from right to left or conversely.

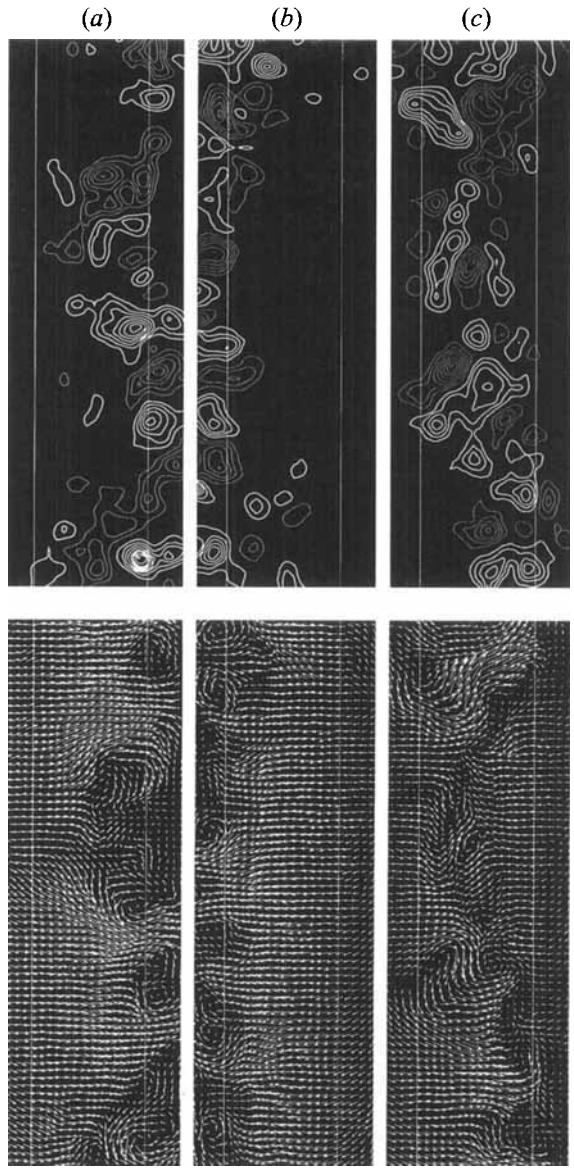

FIGURE 9. Streamwise vorticity and velocity fields near Kármán vortex formation: $x/D = 1$, $Re = 10 \times 10^3$. Minimum vorticity contour level $|\omega_{min}| = 5\ s^{-1}$, contour increment $\Delta\omega = 5\ s^{-1}$.

At larger values of x/D, however, it is possible to observe several classes, or modes, of distortion along the span of the near wake. These distortions have large scales, i.e. long spanwise scales, relative to the spanwise wavelength between vorticity concentrations ω_x. In order to illustrate these distortions, we include images corresponding to $Re = 5 \times 10^3$ (Chyu 1995), as well as $Re = 10 \times 10^3$. Considering, first, figure 8, more specifically images (*a*) and (*b*) at $x/D = 1$, generally uniform patterns of cross-flow from left to right (*a*) and right to left (*b*) are evident. This quasi-uniform sweeping of flow across the wake is associated with particularly well-defined patterns of instantaneous ω_x, which tend to have an alternating positive and negative sense along the span of the cylinder. The patterns shown in images (*c*) and (*d*) are, however, more

complex. In (*c*), the vectors are oriented predominantly to the right in the upper half of the image and to the left in the lower half, corresponding to a nearly discontinuous 'shear' mode, already suggested in the vorticity contours of figure 5. This type of mode is more sharply defined in image (*d*). At the spanwise location designated by the brackets immediately to the right of images (*c*) and (*d*), a particularly large concentration of vorticity forms. These types of large-scale modes, among others, can occur intermittently, and over a range of x/D in the near wake, as the location of the initial Kármán vortex drifts up- and downstream over a large number of cycles.

Generally similar modes occur at the higher Reynolds number $Re = 10 \times 10^3$. In figure 9, corresponding to $x/D = 1$, images (*a*) and (*b*) correspond to sweeping of flow across the wake to the right and left respectively; again, this sweeping effect is associated with the large-scale Kármán vortex formation. The concentrations of streamwise vorticity along the span of the cylinder are quite ordered in both images (*a*) and (*b*). They exhibit a spanwise wavelength of the order of one cylinder diameter. In image (*c*), a shear-type mode involves vectors predominantly to the right in the bottom and top regions of the velocity image, and to the left in the mid-portion of the image. Large-scale concentrations of streamwise vorticity ω_x occur at the locations where the cross-flow changes direction, indicated by the brackets.

7. Overview of near-wake structure and concluding remarks

Over the range of Reynolds number from 5×10^3 to 10×10^3, the streamwise wavelength λ_{VK} between Kármán vortices is an order of magnitude larger than the K–H wavelength λ_{KH} between successive small-scale concentrations of spanwise vorticity ω_z formed in the shear layers separating from the cylinder. Correspondingly, the spanwise wavelengths λ_z of the concentrations of streamwise vorticity ω_x are small in the region where only the K–H vortices exist, relative to values of λ_z where the Kármán vortices dominate. In addition, a third, much larger scale of three-dimensionality occurs; it involves several possible classes, or modes, of distortion; the most pronounced is a severe, nearly discontinuous pattern of ω_x associated with the Kármán vortices.

The three-dimensional features of the near-wake are defined in terms of: circulation of concentrations of streamwise vorticity ω_x; characteristic spanwise λ_z and cross-stream λ_y wavelengths between ω_x concentrations, as determined from spatial correlation of instantaneous ω_x concentrations; and large-scale distortions of patterns of ω_x concentrations. It is demonstrated herein, for both values of Reynolds number, that the spanwise wavelength λ_z rapidly increases from its value at the base of the cylinder to attain a value of the order of the cylinder diameter. It is, however, important to consider simultaneously the variation of the cross-stream wavelength λ_y when interpreting this variation of spanwise wavelength λ_z; in fact, the ratio of λ_y/λ_z can be as high as 0.2 to 0.5, emphasizing the staggered form of the patterns of ω_x. Moreover, the insight gained by considering the instantaneous distributions of streamwise vorticity is highlighted by comparison with root-mean-square distributions; the latter reveals relatively little, due to the non-stationary nature of the ω_x concentrations from cycle to cycle of the near-wake vortex formation.

Figure 10 provides an overview of the quasi-two-dimensional streamline patterns in relation to the instantaneous concentrations of ω_x at $Re = 10 \times 10^3$. Specification of this two-dimensional topology is central to interpreting the generation of three-dimensionality. Irrespective of whether one considers successive K–H or Kármán vortices, it is generally acknowledged that the strain field in the vicinity of the saddle

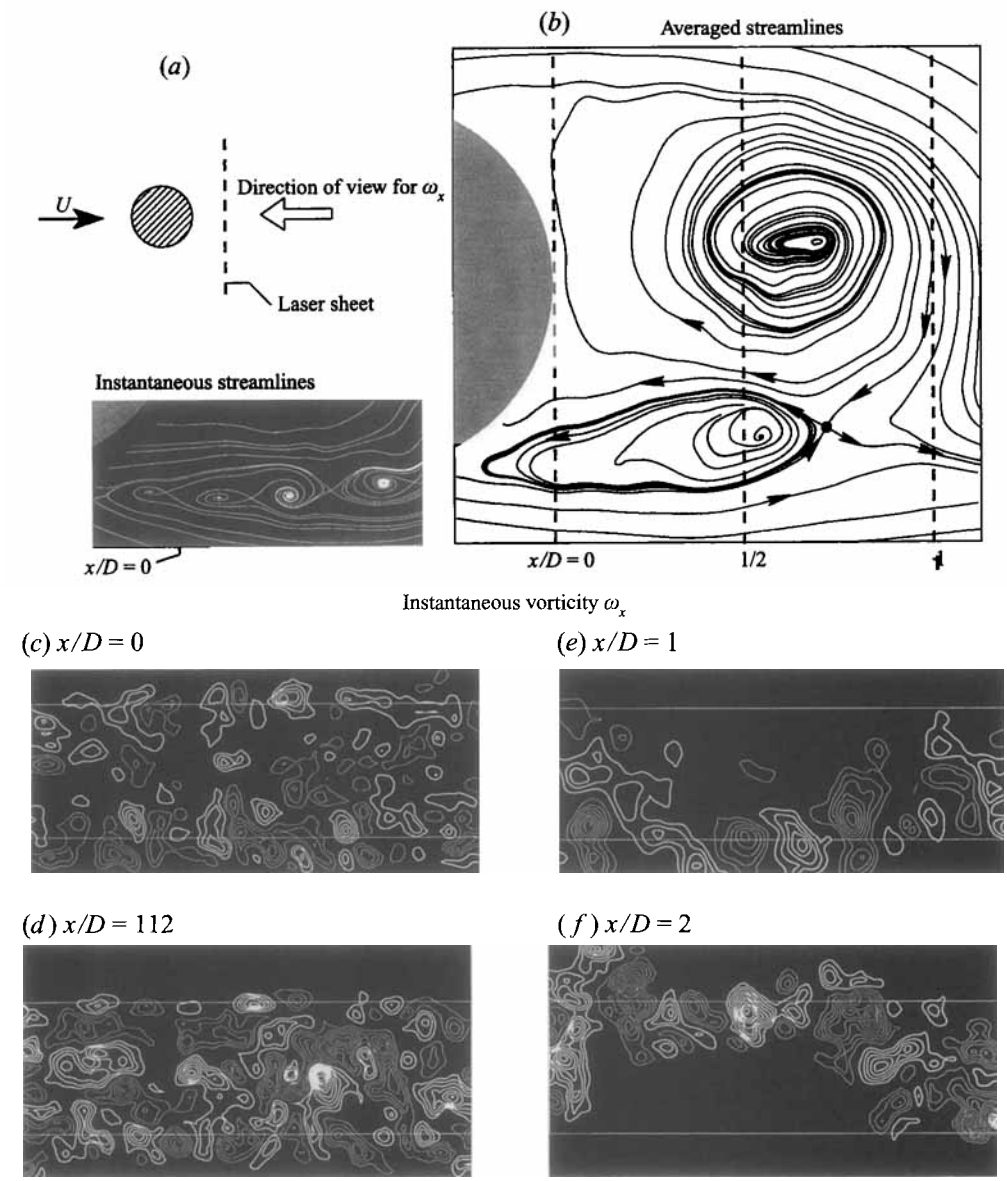

FIGURE 10. Interpretation of instantaneous patterns of streamwise vorticity ω_x in relation to the quasi-two-dimensional streamline topology at $Re = 10 \times 10^3$.

point between vortices is central to the generation of streamwise vorticity. Identification of the saddle point structure is therefore insightful, as evident in the descriptions of mixing layers by Corcos & Lin (1984) and vortex streets by Cantwell & Coles (1983) and Wu, Sheridan & Welsh (1994*c*).

Figure 10(*a*) shows the instantaneous streamline topology of the separating shear layer from the bottom surface of the cylinder; this topology is in a frame moving at three-quarters the free-stream velocity. The occurrence of saddle points between successive vortices is evident. The streamline patterns near the vortex centres all exhibit

spiral patterns, signifying spanwise three-dimensionality; most of these spirals are outward, corresponding to unstable foci. Owing to lack of phase coherence of this vortex system, its structure is smoothed out over a number of Kármán cycles, and it is not detectable in the pattern of figure 10(*b*), which was constructed by averaging five phase-referenced images of the large-scale vortex formation. The phase reference corresponded to the appearance of the centre of the upper large-scale vortex at the same spatial location. The saddle point is designated by the bold dot. According to the interpretation of Wu *et al.* (1994*b*), spanwise disturbances moving along streamlines toward the saddle point will, upon encountering the saddle, be stretched along the streamlines oriented away from the saddle. We emphasize, however, that the complete mechanism giving rise to the remarkably coherent patterns of ω_x is not conclusively resolved. Zhang, Noack & Eckelmann (1994) describe a centrifugal instability in the form of Görtler vortices in the very near wake, based on a direct numerical simulation. An analogous (Rayleigh) centrifugal instability has been computed using a large-eddy simulation for the case of an isolated vortex by Sreedhar & Ragab (1994). These simulations exhibit patterns of streamwise vorticity having several features in common with the present observations.

In the following, we categorize the streamwise evolution of representative patterns of ω_x with reference to figures 10(*a*) and 10(*b*).

Kelvin–Helmholtz vortex region. Immediately downstream of separation from the cylinder, the pattern of ω_x is as indicated in figure 10 (*a*). The cross-flow plane, which touches the base of the cylinder, i.e. $x/D = 0$, also lies between the first and second saddle points of the K–H vortex system, so significant levels of ω_x should be evident. As is indicated in figure 10(*c*), showing instantaneous ω_x, the degree of development of the three-dimensionality and level of vorticity concentration are substantially more advanced in the lower than in the upper shear layer; this corresponds to earlier onset and development of the quasi-two-dimensional small-scale vortices in the upper layer, illustrated in figure 2. The staggered pattern of small-scale concentrations of ω_x shown in the lower layer of image (*c*) has certain features in common with those formed in the high Reynolds number mixing layer from a thin plate (Bell & Mehta 1992). The complexity of the ω_x pattern is no doubt influenced by the upstream recirculation of stretched vorticity from the saddle point shown in figure 10 (*b*). The ratio of the averaged spanwise λ_z to streamwise λ_x (quasi-two-dimensional) wavelength, λ_z/λ_x, is of the order of 2, which is in good agreement with the initial region of development of mixing layers at higher Reynolds number characterized by Huang & Ho (1990) and Bell & Mehta (1992). Unlike the classical mixing layer, the adjacent small-scale vortices on the shear layer from the cylinder do not generally undergo coalescence, perhaps due to the existence of the quasi-two-dimensional recirculation zone of image (*b*); there is, therefore, no mechanism for decreasing the ratio λ_z/λ_x for increasing x.

Evaluation of the instantaneous dimensionless circulation $\Gamma^* \equiv \Gamma_x/\pi UD$ of the ω_x concentrations at $x/D = 0$ gives average and maximum values of 0.03 and 0.07 respectively. These values compare with the instantaneous maximum circulation $\Gamma_z^* \approx 0.15$ of the small-scale spanwise vorticity ω_z concentrations shown in figure 2.

Base flow region. Immediately downstream of the base of the cylinder, at $x/D = 1/2$, patterns of streamwise vorticity ω_x are not simply confined to the separating shear layers; rather, concentrations of substantial scale and strength exists across the entire near wake, as shown in figure 10 (*d*). The rich array of ω_x concentrations in the base region occurs well upstream of the saddle point shown in figure 10(*b*). The degree to which this array of ω_x is due to (i) an upstream consequence of vortex stretching, (ii)

further manifestation of a centrifugal instability, or a combination of (i) and (ii), remains unresolved.

Evaluation of the spanwise and cross-stream wavelengths λ_z and λ_y over the entire cross-section of the near wake shows instantaneous and averaged values significantly larger than those at $x/D = 0$ (see figure 6). On the basis of this instantaneous image, it is difficult to distinguish those ω_x concentrations strictly associated with the shear layers from those in the base (central) portion of the wake. Close inspection of figure 10(*d*), however, indicates generally smaller-scale ω_x concentrations along the lower boundary than along the centre of the wake, corresponding respectively to the shear-layer and base regions. This observation suggests, in a simplified sense, that the pattern of ω_x in the shear layer tends to retain its identity in the very near wake. The potential communication between regions of ω_x in the shear layer and base region, however, provides a much more complicated system of ω_x than exists in an isolated mixing layer.

The outer boundaries of the wake represented in figure 10(*d*) change insignificantly with time, i.e. during formation of the Kármán vortex, suggested not only by figure 10(*d*), but also by images corresponding to $x/D \leqslant 1/2$ in figure 5. This region of the wake of located sufficiently far upstream of the saddle point such that large-scale cross-stream undulations of the entire wake are not detectable.

Kármán vortex region. Immediately downstream of the saddle point, at the location $x/D = 1$, represented by figure 10(*e*), it is possible to identify particularly ordered large-scale concentrations of streamwise vorticity ω_x. The location of the ω_c concentrations along the bottom of figure 10(*e*) is consistent with the location of the streamline emanating from the saddle point at the bottom of figure 10(*b*). The spanwise wavelength λ_z of the ω_x concentrations is of the order of the cylinder diameter D, and their average and maximum values of circulation Γ_x^* are 0.06 and 0.26 respectively, two to three times larger than the corresponding values of Γ_z^* for the small-scale K–H vortices in the shear layers from the cylinder. The peak value of $\Gamma_x^* = 0.26$ is, however, significantly smaller than the instantaneous Γ_z^* of the spanwise Kármán vortices, which is of the order unity, i.e. $\Gamma_z^* \sim 1$.

During formation of the Kármán vortex, the entire pattern of ω_x concentrations is swept across, i.e. moves from one side to the other of, the cross-flow plane. The type of instantaneous pattern shown in figure 10(*e*) occurs at the extreme position of this cross-stream oscillation. Note that the plane at $x/D = 1$ is approximately parallel to streamlines that originate from the irrotational region exterior to the wake, and extend across the wake. This streamline pattern, relative to the laser sheet at $x/D = 1$, corresponds to the pattern of the uniform velocity extending over the cross-flow plane in figures 8 and 9.

Distorted Kármán vortex region. Near and downstream of the first saddle point, the spanwise structure of the wake intermittently exhibits large-scale distortions of the patterns of ω_x. Such distortions are represented by figure 10(*f*), which, in this case, is estimated to occur at the second saddle point on the upper side of the wake. This distortion involves a remarkably abrupt, nearly discontinuous, change in the location of the ω_x concentrations. The *y*-shaped connections between spanwise vortices observed in the smoke visualization studies of Norberg (1993), at a Reynolds number of 5.5×10^3, would correspond to the essentially discontinuous distortions of the patterns of ω_x presented here. A large-scale concentration of ω_x is present at the location of the so-called discontinuity, evident not only in figure 10(*f*), but also in figures 8 and 9 at the locations of the brackets. At this location, there is an abrupt change in the nominal direction of the velocity across the wake such that the overall velocity pattern in the vicinity of the discontinuity exhibits a shear-type flow. At very low values of *Re*, of the

order of a few hundred, the qualitative visualizations of Gerrard (1978) and Williamson (1989) suggest isolated regions of streamwise vorticity at dislocations in patterns of Kármán vortices otherwise free of ω_x concentrations. The nearly abrupt large-scale distortions of interest here, with a pronounced concentrations of ω_x at the spanwise location of the so-called discontinuity, may be akin to the dislocation phenomenon observed at low Reynolds number. This aspect deserves further study.

The authors are indebted to Drs Jung-Chang Lin and John Sheridan for fruitful discussions. The support of the Office of Naval Research under Grants N00014-94-1-0185 and N00014-90-J-1510, as well as the National Science Foundation under Grant CTS 8922095, is gratefully acknowledged.

REFERENCES

BAYS-MUCHMORE, B. & AHMED, A. 1993 On streamwise vortices in turbulent wakes of cylinders. *Phys. Fluids* A **5**, 387–392.

BELL, J. H. & MEHTA, R. D. 1992 Measurements of the streamwise vortical structures in a plane mixing layer. *J. Fluid Mech.* **239**, 213–248.

BERNAL, L. P. & ROSHKO, A. 1986 Streamwise vortex structure in plane mixing layers. *J. Fluid Mech.* **170**, 499–525.

BLOOR, M. S. 1964 The transition to turbulence in the wake of a circular cylinder. *J. Fluid Mech.* **19**, 290–304.

BREIDENTHAL, R. 1981 Structure in turbulent mixing layers in wakes using a chemical reaction. *J. Fluid Mech.* **109**, 1–24.

BROWN, G. L. & ROSHKO, A. 1974 On density effects in large structures in turbulent mixing layers. *J. Fluid Mech.* **64**, 775–816.

CANTWELL, B. & COLES, D. 1983 An experimental study of entrainment and transport in the turbulent near wake of a circular cylinder. *J. Fluid Mech.* **136**, 321–374.

CHYU, C.-K. 1995 A study of the near-wake structure for a circular cylinder. PhD Dissertation, Department of Mechanical Engineering and Mechanics, Lehigh University.

CORCOS, G. M. & LIN, S. J. 1984 The mixing layer: deterministic models of a turbulent flow. Part 2. The origin of the three-dimensional motion. *J. Fluid Mech.* **139**, 67–95.

FILLER, J. R., MARSTON, P. L. & MIH, W. C. 1991 Response of the shear layer separating from a circular cylinder to small-amplitude rotational oscillations. *J. Fluid Mech.* **231**, 481–499.

GERRARD, J. H. 1978 The wakes of cylindrical bluff body at low Reynolds number. *Phil. Trans. R. Soc. Lond.* A **228**, 351–382.

HAMA, F. R. 1957 Three-dimensional vortex pattern behind a circular cylinder. *J. Aero. Sci.* Feb., 156–158.

HAYAKAWA, M. & HUSSAIN, F. 1989 Three-dimensionality of organized structures in a plane turbulent wake. *J. Fluid Mech.* **206**, 375–404.

HO, C. M. & HUERRE, P. 1984 Perturbed free shear layers. *Ann. Rev. Fluid Mech.* **16**, 365–424.

HUANG, L.-S. & HO, C.-M. 1990 Small scale transition in a plane mixing layer. *J. Fluid Mech.* **210**, 475–500.

HUSSAIN, A. K. M. F. 1986 Coherent structures in turbulence. *J. Fluid Mech.* **173**, 303–356.

JIMENEZ, J., COGOLOS, M. & BERNAL, L. P. 1985 A perspective view of the plane mixing layer. *J. Fluid Mech.* **152**. 125–143.

KÖNIG, M., EISENLOHR, H. & ECKELMANN, H. 1993 Visualization of the spanwise cellular structure of the laminar wake of wall-bounded circular cylinders. *Phys. Fluids* A **4**, 869–872.

KONRAD, J.-H. 1976 An experimental investigation of mixing in two-dimensional turbulent shear flows with applications to diffusion-limited chemical reactions. *Internal Rep.* CJIT-8-PU. California Institute of Technology.

KOURTA, A., BOISSON, H. C., CHASSING, P. & HA MINH, H. 1987 Nonlinear interaction and the transition to turbulence in the wake of a circular cylinder. *J. Fluid Mech.* **81**, 141–161.

LASHERAS, J. C., CHO, J. S. & MAXWORTHY, T. 1986 On the origin and evolution of streamwise vortical structure in a plane free-shear layer. *J. Fluid Mech.* **172**, 231–258.

LASHERAS, J.-C. & CHOI, H. 1988 Three-dimensional instability of a plane free shear layer; an experimental study of the formation and evolution of streamwise vortices. *J. Fluid Mech.* **189**, 53–86.

LIN, J.-C. & ROCKWELL, D. 1994 Cinematographic system for high-image-density particle image velocimetry. *Exps. Fluids* **17**, 110–118.

LIN, J.-C., TOWFIGHI, J. & ROCKWELL, D. 1995 Instantaneous structure of near-wake of a circular cylinder: on the effect of Reynolds number. *J. Fluids Struc.* **9**, 409–418.

LIN, J.-C., VOROBIEFF, P. & ROCKWELL, D. 1993 Cinematographic system for high-image-density particle image velocimetry. *Bull. Am. Phys. Soc.*, **38**, Abs. IG3, 301.

LIN, J.-C., VOROBIEFF, P. & ROCKWELL, D. 1995 Three dimensional patterns of streamwise vorticity in the turbulent near-wake of a cylinder. *J. Fluids Struc.* **9**, 231–234.

LIN, J.-C., VOROBIEFF, P. & ROCKWELL, D. 1996 Space-time imaging of a near-wake by high-image-density particle image cinematography. *Phys. Fluids* **8**, 555–564.

MANSY, H., YANG, P. M. & WILLIAMS, D. R. 1994 Quantitative measurements of three-dimensional structures in the wake of a circular cylinder. *J. Fluid Mech.* **20**, 277–296.

MEINHART, C. D., PRASAD, A. K. & ADRIAN, R. J. 1992 Parallel digital processor system for particle image velocimetry. *Proc. Sixth Intl Symp. on Applications of Laser Techniques to Fluid Mechanics, Lisbon, Portugal*, pp. 30.1.1–30.1.6.

NORBERG, C. 1993 Pressure forces on a circular cylinder in cross flow. In *Bluff-Body Wakes, Dynamics and Instabilities* (ed. H. Eckelmann, J. M. R. Graham, P. Huerre & P. A. Monkewitz), *Proc. IUTAM Symp., Göttingen, German, Sept. 7–11, 1992*, pp. 275–278. Springer.

NORBERG, C. 1994 An experimental investigation of the flow around a circular cylinder: influence of aspect ratio. *J. Fluid Mech.* **258**, 287–316.

ROCKWELL, D. 1993 Quantitative visualization of bluff-body wakes by particle image velocity. In *Bluff-Body Wakes, Dynamics and Instabilities* (ed. H. Eckelmann, J. M. R. Graham, P. Huerre & P. A. Monkewitz), *Proc. IUTAM Symp., Göttingen, Germany, Sept. 7–11, 1992*, pp. 263–270. Springer.

ROCKWELL, D. & LIN, J.-C. 1993 Quantitative interpretation of complex, unsteady flows via high-image-density particle image velocimetry. In *Optical Diagnostics in Fluid and Thermal Flow, Proc.* SPIE (*Intl Soc. Optical Engng*), vol. 2005, pp. 490–503.

ROCKWELL, D., MAGNESS, C., ROBINSON, O., TOWFIGHI, J., AKIN, O., GU, W. & CORCORAN, T. 1992 Instantaneous structure of unsteady separated flows via particle image velocimetry. *Rep.* PI-1. Fluid Mech. Lab., Dept. Mech. Engng & Mech., Lehigh University.

ROCKWELL, D., MAGNESS, C., TOWFIGHI, J., AKIN, O. & CORCORAN, T. 1993 High-image-density particle image velocimetry using laser scanning techniques. *Exps. Fluids* **14**, 181–192.

ROSHKO, A. 1976 Structure of turbulent shear flows: a new look. *AIAA J.* **14**, 1349–1357.

SHERIDAN, J., SORIA, J., WU, J. & WELSH, M. C. 1993 The Kelvin–Helmholtz instability of the separated shear layer from a circular cylinder. In *Bluff-Body Wakes, Dynamics and Instabilities* (ed. H. Eckelmann, J. M. Graham, P. Huerre & P. A. Monkewitz), *Proc. IUTAM Symp., Göttingen, Germany, Sept. 7–11, 1992*, pp. 115–117. Springer.

SZEPESSY, S. & BEARMAN, P. W. 1992 Aspect ratio and end plate effects on vortex shedding from a circular cylinder. *J. Fluid Mech.* **234**, 191–217.

TOWFIGHI, J. & ROCKWELL, D. 1994 Flow structure from an oscillating nonuniform cylinder: generation of patterned vorticity concentrations. *Phys. Fluids.* **6**, 531–546.

UNAL, M. F. & ROCKWELL, D. 1988 On vortex formation from a cylinder. Part 1. The initial instability. *J. Fluid Mech.* **190**, 491–512.

WEI, T. & SMITH, C. R. 1986 Secondary vortices in the wake of circular cylinders. *J. Fluid Mech.* **169**, 513–533.

WILLIAMSON, C. H. K. 1988 The existence of two stages in the transition to three-dimensionality of a cylinder wake. *Phys. Fluids* **31**, 3165–3168.

WILLIAMSON, C. H. K. 1989 Oblique and parallel modes of vortex shedding in the wake of a circular cylinder at low Reynolds numbers. *J. Fluid Mech.* **206**, 574–627.

WILLIAMSON, C. H. K. 1992 The natural and forced formation of spot-like 'vortex dislocations' in the transition of a wake. *J. Fluid Mech.* **243**, 393–441.

WILLIAMSON, C. H. K. 1996 Vortex dynamics in the cylinder wake. *Ann. Rev. Fluid Mech.* **28**, 477–539.

WILLIAMSON, C. H. K., WU, J. & SHERIDAN, J. 1995 Scaling of streamwise vortices in wakes. *Phys. Fluids* **7**, 2307–2310.

WU, J., SHERIDAN, J., HOURIGAN, K., WELSH, M. C. & THOMPSON, M. 1994*a* Longitudinal vortex structures in a cylinder wake. *Phys. Fluids* **6**, 2883–2885.

WU, J., SHERIDAN, J., SORIA, J. & WELSH, M. C. 1994*b* An experimental investigation of streamwise vortices in the wake of a bluff body. *J. Fluids Struct.* **8**, 621–635.

WU, J., SHERIDAN, J. & WELSH, M. C. 1994*c* Vortex filament simulation of the longitudinal vortices found in the wake of a bluff body. In *Boundary Layer and Free-Shear Flows*. ASME FED, vol. 184, pp. 187–194.

WU, J., SHERIDAN, J., WELSH, M. C., HOURIGAN, K., SORIA, J. & THOMPSON, M. 1994*d* Shear layer vortices and longitudinal vortices in the wake of a circular cylinder. *Proc. Int. Colloq. on Jet, Wakes and Shear Layers, Melbourne, Australia, 18–20 April 1994.*

YOKOI, Y. & KAMEMOTO, K. 1992 Initial state of a three-dimensional vortex structure existing in a two-dimensional boundary layer separation flow (observation of laminar boundary layer separation over a circular cylinder by flow visualization. *Japanese Soc. Mech. Engng. Int. J.* H **35**, 189–195.

YOKOI, Y. & KAMEMOTO, K. 1993 Initial stage of a three-dimensional vortex structure existing in a two-dimensional boundary layer separation flow (visual observation of laminar boundary-layer separation over a circular cylinder from the side of a separated region). *Japanese Soc. Mech. Engng Intl J.*, H **36**, 201–206.

ZHANG, H.-Q., FEY, U., NOACK, B. R., KÖNIG, M. & ECKELMANN, H. 1995 On the transition of the cylinder wake. *Phys. Fluids* **7**, 779–794.

ZHANG, H.-Q., NOACK, B. R. & ECKELMANN, H. 1994 Numerical computation of the 3-D cylinder wake. *Max-Planck-Institut für Strömungsforschung Göttingen*, Rep. 3/1994.